INSTITUTE OF PHYSICS PUBLISHING JOURNAL OF PHYSICS B: ATOMIC, MOLECULAR AND OPTICAL PHYSICS

J. Phys. B: At. Mol. Opt. Phys. **37** (2004) 1893–1907 PII: S0953-4075(04)72135-5

Direct measurement of P^+ for electron impact excitation of H(2p) at 54.4 eV

M L Gradziel and R W O'Neill

Department of Experimental Physics, National University of Ireland, Maynooth, Co. Kildare, Republic of Ireland

E-mail: Marcin.Gradziel@may.ie

Received 13 November 2003, in final form 22 March 2004
Published 23 April 2004
Online at stacks.iop.org/JPhysB/37/1893 (DOI: 10.1088/0953-4075/37/9/010)

Abstract

We report results of direct measurements of the reduced Stokes parameters $\bar{P}_1$, $\bar{P}_2$ and $\bar{P}_3$ for electron impact excitation of H(2p) at 54.4 eV over the scattering range 10–40°. These three parameters have been measured simultaneously for the first time using a VUV double-rotation polarization analyser consisting of a MgF_2 retarder followed by a SiO_2 reflection linear polarizer. As expected, our measurements for $\bar{P}_1$ and $\bar{P}_2$ are in good agreement with theoretical calculations and previous experimental data. Our data for $\bar{P}_3$ differ significantly from previous experimental measurements and theoretical calculations. Consequently, we find that the coherence parameter P^+ deviates significantly from unity at 30°. If correct, this signifies that spin-exchange scattering may be more important than has previously been thought.

1. Introduction

The electron–photon delayed coincidence technique has been used since 1974 to investigate the coherence properties of atomic decay radiation. Coincident detection of an electron which has been scattered into a well-defined direction and the corresponding decay photon permits a subensemble of the total excited atomic decay radiation to be selected for examination. Two complementary techniques have been used: (i) *polarization correlation* measures the polarization properties of the coincident photon flux in some fixed direction, and (ii) *angular correlation* maps the intensity variation of the coincident decay radiation as a function of photon emission direction. In principle, these types of measurement provide a highly detailed test of scattering theories; in practice, the measurements are challenging and are frequently subject to large statistical uncertainties, particularly at large electron scattering angles.

There has generally been excellent agreement between experiment and theory describing the scattering of electrons by helium [1] and light alkali atoms (Li, Na) [2–5]. Since 1998 there has also been a consensus that electron impact excitation of atomic hydrogen at the

benchmark energy of 54.4 eV is well understood. This consensus followed publication of angular correlation measurements of Yalim *et al* [6, 7], and linear polarization correlation measurements of O'Neill *et al* [8]. Both of these groups investigated electron scattering from atomic hydrogen at angles above 100°. Both data sets contradicted the earlier angular correlation data of Williams [9] and Weigold *et al* [10], and both supported the trend of theoretical predictions [11–15]. The angular correlation data of Yalim *et al* were in excellent agreement with convergent close coupling (CCC) calculations, while the Stokes parameters measured by O'Neill *et al* fell somewhat below CCC predictions, but supported the theoretical trend. The picture emerging was that experiment and theory were in broad agreement and that the hydrogen problem was solved.

Measurements of the circular polarization have been reported by Williams [16] and Nic Chormaic *et al* [17]. These data are somewhat problematic: they are not in agreement with each other, and only the Williams data are consistent with theoretical predictions. Williams measured the circular polarization using a double-reflection polarization analyser: he obtained results over the scattering range 10–150° that were consistent with theoretical models, but with large statistical uncertainties (typically ±15% at one standard deviation). Nic Chormaic *et al* used a MgF_2 retarder and a silica mirror polarizer and published $\bar{P}_3$ values in the 5–40° range. Their data showed essentially flat angular dependence and values generally close to zero, with relatively small error bars. This result was in complete disagreement with theoretical predictions and the data of Williams, and was largely ignored by the theoretical community.

We report here the first simultaneous measurements of all three Stokes parameters characterizing the Lyman-α decay radiation (121.6 nm) resulting from electron impact excitation of H(2p) at an incident energy of 54.4 eV and in the range of electron scattering angles 4–40°. These measurements allowed us for the first time to determine the important excitation coherence parameter P^+ [18] in a single self-consistent measurement.

2. Experimental method

The density matrix that describes electron impact excitation of the 2^2P_J states of hydrogen is specified by three independent parameters in addition to the angular differential scattering cross-section σ. These have traditionally been taken as

$$\lambda = \frac{\langle |a_0|^2 \rangle}{\sigma} \qquad R = \frac{\mathrm{Re}\langle a_1 a_0^* \rangle}{\sigma} \qquad I = \frac{\mathrm{Im}\langle a_1 a_0^* \rangle}{\sigma}, \tag{1}$$

where the brackets denote an average over unobserved electron spins of the transition amplitudes a_M for different magnetic substates $|\mathrm{LM}\rangle$ of the excited ^2P_J state. An equivalent parametrization is given by the set of so-called reduced Stokes parameters $\bar{P}_i$, which also describe the nascent excited charge cloud, i.e. immediately following instantaneous excitation at $t = 0$. These two sets are related by [18]

$$\bar{P}_1 = 2\lambda - 1 \qquad \bar{P}_2 = -2\sqrt{2}R \qquad \bar{P}_3 = 2\sqrt{2}I. \tag{2}$$

The reduced Stokes parameters $\bar{P}_i$ can be deduced from the values of experimentally measured Stokes parameters P_i, provided that account is taken of the depolarization inherent in the evolution of the excited state under the influence of the internal forces over its lifetime ($\tau = 1.6$ ns). As far as the two equivalent experimental techniques are concerned, measurements of angular correlations in the scattering plane, without regard to polarization analysis of the radiation, yield values for only two independent parameters: λ and R.

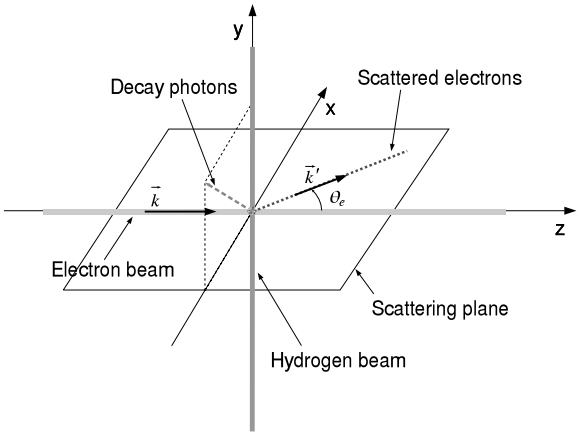

Figure 1. Schematic diagram of the experimental geometry.

A measurement of the circular polarization P_3 of the decay radiation is required to specify I. The excitation coherence parameter P^+ is given by

$$P^+ = \sqrt{\bar{P}_1{}^2 + \bar{P}_2{}^2 + \bar{P}_3{}^2}, \tag{3}$$

and its determination requires a measurement of all three reduced Stokes parameters.

2.1. Experimental setup

Our experimental geometry is shown in figure 1, the co-ordinate frame shown being the so-called *collision frame*. The momenta of the incident primary electrons $\vec{k}$ and detected scattered electrons $\vec{k}'$ respectively define the scattering plane. Emitted photons are detected in a direction at 90° to $\vec{k}$ and at an elevation angle of 135° to the scattering plane, i.e. $\theta = 90°$, $\phi = 135°$ in the collision frame. Lyman-α radiation from the hydrogen source prevents positioning of the polarization analyser at the preferred position perpendicular to the scattering plane ($\theta = 90°, \phi = 90°$).

The general expressions relating the reduced Stokes parameters $\bar{P}_i$ to experimentally measured Stokes parameters P_i for radiation propagating in the direction (θ, ϕ) can be obtained using equations (4.3.11) of Blum and Kleinpoppen [19] and conversion factors for state multipoles and independent parameters given by Andersen *et al* [18]. A series of purely algebraic substitutions gives two equations which, for the particular analysis direction specified reduce to

$$\bar{P}_1 = \frac{25P_1 - 3}{3(3 - P_1)} \qquad \bar{P}_2 = \frac{6\sqrt{2}P_2}{3 - P_1} \qquad \bar{P}_3 = \frac{18\sqrt{2}P_3}{7(3 - P_1)}. \tag{4}$$

The only practical difficulty of using this detection direction is that two Stokes parameter measurements are required to determine each of $\bar{P}_2$ and $\bar{P}_3$, since these also depend on P_1.

The basic apparatus used in the present experiment is similar to that used previously in this laboratory [8, 17], although substantial improvements and re-testing were implemented for this work. A thermal beam of deuterium atoms produced by the dissociation of molecular deuterium in an RF discharge is intersected by an electron beam of energy 54.4 eV (energy spread approximately 0.5 eV) and diameter ∼1 mm. Deuterium is preferred as target in order to minimize the small effect of hyperfine structure on the post-collisional evolution of the

excited state. For this isotope the hyperfine effects are negligible in the derivation of the reduced Stokes parameter relations. The discharge source provides a steady-state dissociation fraction of ~60% and an atomic density at the interaction point of $\sim 3 \times 10^{11}$ cm^{-3} at a source pressure of approximately 0.07 Torr. Electrons scattered into a well-defined angle are selected for an energy loss of 10.2 eV, corresponding to $n = 2$ excitation, using two consecutive 127° electrostatic analysers. Great care has been taken to shield the interaction region from stray electric fields to avoid quenching of the H(2s) state. The circular entrance aperture of the electron energy analyser subtends a solid angle at the interaction region of $\sim 9 \times 10^{-4}$ sr (reduced to 7×10^{-5} sr for $\theta_e \leqslant 10°$). Lyman-α photons emitted in the detection direction are collected by a VUV polarization analyser and detected by a channel electron multiplier coated with CsI, which enhances the Lyman-α detection efficiency.

2.2. Determination of the coincidence rate

The electron–photon delayed coincidence spectrum consists of a coincidence peak superimposed on a background of random coincidences. The area under the coincidence peak is the useful coincidence signal. Typically, one would determine the area under the peak by summing coincidence counts in a region encompassing the peak, and then subtract the background calculated by summing counts in a region away from the peak. The background is assumed to be flat [20]. Careful analysis of a typical system, which uses a combination of a time-to-amplitude converter (TAC) and a multichannel analyser to acquire the coincidence spectrum, shows that the background falls off exponentially with a decay constant that depends on the overall photon detection rate. Ignoring this, and assuming that the background is flat, can lead to a systematic error in the measured values of polarization.

In the limit of perfect timing resolution the coincidence peak would also have exponential shape related to the finite lifetime of the H(2p) state (1.6 ns). In reality the timing resolution is finite and can be quantified in terms of an appropriate apparatus function. The shape of the observed coincidence peak is a result of a convolution of this function with the lifetime-related exponential component. We use channeltron detectors for both electron and photon detection, and their relatively long transit times and pulse widths mean that our timing resolution is far from perfect, and the apparatus function, with an FWHM of 6 ns, dominates. To extract the coincidence detection probability from the measured spectra we have developed a model spectrum whose parameters we fit to the actual data (see figure 2).

It can be shown that under simplifying assumptions that can be applied to a typical coincidence measurement, namely that the probability of detection of the correlated photon is low, and that the coincidence rate changes slowly within a single MCA channel, the number of coincidence counts $C(n)$ in channel n of the MCA is given by

$$C(n) = \left\{ \frac{\bar{\eta}(\vec{\alpha})}{2\tau} \exp\left(-\frac{\left(n+\frac{1}{2}\right)W - \Delta t}{\tau} + \frac{\sigma_a^2}{4\tau^2} \right) \left[1 + \operatorname{erf}\left(\frac{\left(n+\frac{1}{2}\right)W - \Delta t}{\sigma_a} - \frac{\sigma_a}{2\tau} \right) \right] + \dot{N}_{\mathrm{ph}}(\vec{\alpha}) \right\} \exp\left(-\dot{N}_{\mathrm{ph}}(\vec{\alpha}) \left(n + \frac{1}{2} \right) W \right) W N_{VS}, \tag{5}$$

where $\bar{\eta}(\vec{\alpha})$ is the coincidence signal and $N_{\mathrm{ph}}(\vec{\alpha})$ is the total count rate in the photon channel. Both depend on the polarization analyser setting $\vec{\alpha}$. The σ_a parameter is the Gaussian width of the apparatus function, while τ combines the effect of the finite lifetime of the excited state and possible small asymmetry of the apparatus function. W is the width of an MCA channel and Δt is a delay related to the particular choice of the position of zero on the time axis. N_{VS} is the number of valid starts of the TAC.

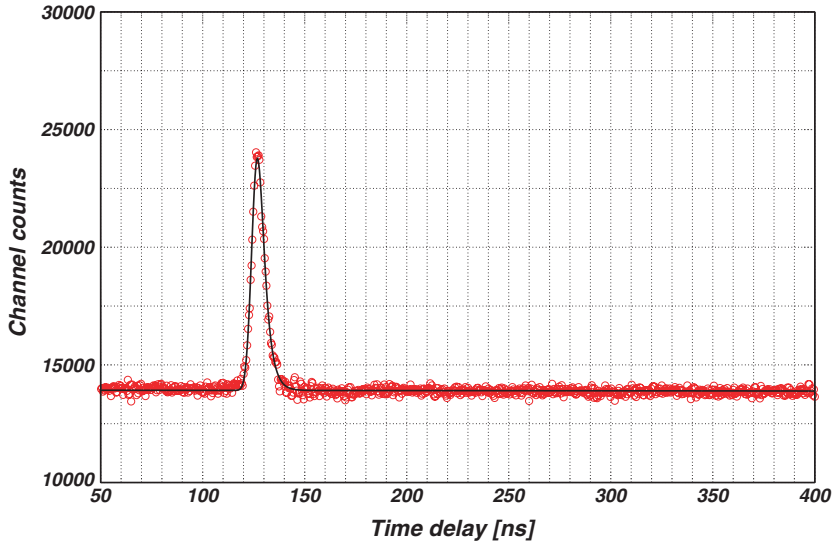

Figure 2. A sample scattered electron-decay photon coincidence spectrum with fitted model distribution.

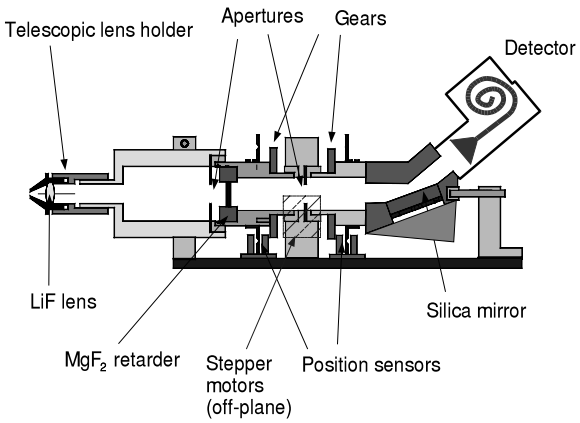

Figure 3. Polarization analyser cross-section.

This method automatically takes care of the problem of the sloping background and ensures that the measured coincidence detection probability is not affected by the arbitrary selection of the regions of interest in the spectrum. Moreover, the statistical uncertainty of the coincidence detection probability determined using this method is reduced by typically 5–20% (for typical acqusition times). Knowing the shape of the peak allows us to determine its area more accurately.

2.3. Polarization analyser

The polarization analyser shown in figure 3 is a new device that was designed and constructed for these studies. It is a double-rotation device, i.e. it comprises a retarder and linear polarization analyser that may be rotated independently.

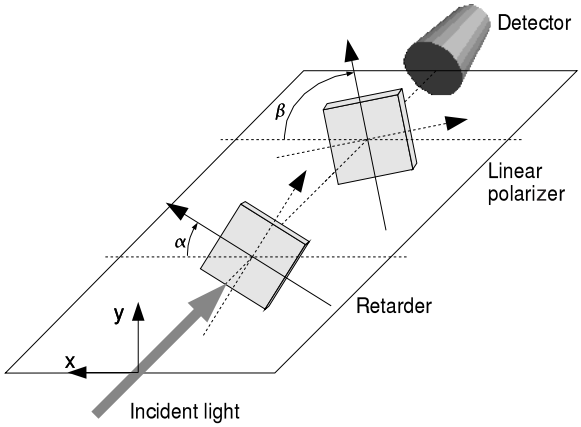

Figure 4. Polarization measurement geometry. The change of the direction of propagation after the reflection linear polarizer is not shown for clarity.

A schematic of the double-rotation polarization analysis is shown in figure 4. The intensity of light reaching the detector is related to the Stokes parameters of the light and the orientation angles of the analyser elements by

$$I(\alpha, \beta) = \frac{I_0 t_p t_r}{P+1}[1 + P(P_1(\cos 2(\beta - \alpha)\cos 2\alpha - \cos\Delta \sin 2(\beta - \alpha)\sin 2\alpha) + P_2(\cos 2(\beta - \alpha)\sin 2\alpha + \cos\Delta \sin 2(\beta - \alpha)\cos 2\alpha) + P_3 \sin\Delta \sin 2(\beta - \alpha))], \quad (6)$$

where I_0 is the light intensity at the analyser entrance, P is the polarization efficiency of the polarizer, defined as the linear polarization of initially unpolarized light, Δ is the phase shift of the retarder (retardance), t_p is the transmittance of the linear polarizer and t_r is the transmittance of the retarder.

The linear polarizing element is a quartz (fused silica) reflector whose polarization efficiency was measured as $P = 86.4 \pm 0.3\%$, using a polariscope arrangement [21]. The retarder is a zero-order MgF_2 waveplate manufactured by Halle Nafl GmbH. We have carefully measured its retardance to be $\Delta = (-84.1 \pm 0.6)^\circ$. It may be of interest to note that it is crucially important to independently verify the retardance of any such device, since it is extremely difficult to engineer accurate retardance values at such short wavelengths. The manufacturer provided us with three nominal quarter-wave plates; the actual retardances of these three units were measured to range from 84 to 167°.

Calibration of the polarization analyser was performed at the wavelength of 121.6 nm, using Lyman-α light from hydrogen atoms excited by collisions with electrons of energy just above the excitation threshold of H(2p). This procedure minimized the contribution from collisionally excited hydrogen molecules, and ensured quasi-monochromaticity of the light used for calibration. More than 99% of the total detected photon flux could be attributed to Lyman-α photons. The finite linear polarization of the photon source, multiplied by the polarization efficiency P, was measured using the instrument being calibrated, without the extra mirror. This measurement, and two extra measurements in the polariscope arrangement—the first with rotation of the second reflector, and the second with the rotation of the retarder—allowed us to fully determine the characteristics of the polarization analyser. The procedure is outlined below.

In a non-coincidence measurement, because of the symmetry of the problem, the light emitted by the excited atoms is partially linearly polarized in the direction of the incident electron beam [19]. In terms of a Stokes vector $\vec{s}_x$ [22], we have

$$\vec{s}_x = I_x \begin{pmatrix} 1 \\ P_1 \\ 0 \\ 0 \end{pmatrix}. \tag{7}$$

In the measurement without the extra mirror, and with the retarder fixed at $\alpha = 0^\circ$, the total intensity of the light transmitted through the analyser, as a function of the orientation of the linear polarizer β, can be shown to be

$$I_1(\beta) = \frac{I_x}{P+1}\{1 + P P_1 \cos(2\beta)\}. \tag{8}$$

Therefore $P P_1$ can be determined from this measurement.

For a measurement in the polariscope geometry, with the polarization axis of the first mirror set parallel to the electron beam, the intensity of the transmitted light is similarly given by

$$I_2(\beta) = \frac{I_x}{(P+1)^2}\{(1 + P P_1) + (P^2 + P P_1)\cos(2\beta)\}, \tag{9}$$

if the second linear polarizer is rotated (angle of rotation β), while the retarder is fixed at $\alpha = 0^\circ$; or by

$$I_3(\alpha) = \frac{I_x}{(P+1)^2}\{(1 + P P_1) + (P^2 + P P_1)[\cos^2(2\alpha) + \cos\Delta \sin^2(2\alpha)]\}, \tag{10}$$

if the second linear polarizer is fixed at $\beta = 0^\circ$, while the retarder is rotated.

The polarization efficiency P can be determined from (9), if $P P_1$ is known (from (8)). Then $\cos\Delta$ can be determined from (10). Therefore only the sign of Δ needs to be additionally established (for example based on manufacturer's data). No assumptions with regards to the actual linear polarization of the light source were necessary.

The polarization analyser was preceded by a LiF lens of focal length 10 mm at 121.6 nm which increases the solid angle subtended by the analyser at the point of intersection of the beams (focal point of lens) to 0.7 sr. The large collection solid angle of the polarization analyser requires that equations (4) be modified to account for this. This was done using the procedure of Goeke *et al* [23] and Humphrey [24] by integrating the analytical expressions for the relevant Stokes parameters over the acceptance solid angle of the detector, given by the opening half-angle $\delta = 28^\circ$, to obtain

$$\bar{P}_1 = \frac{25.72P_1 - 3}{3(3 - 0.936P_1)} \qquad \bar{P}_2 = \frac{6.295\sqrt{2}P_2}{3 - 0.936P_1} \qquad \bar{P}_3 = \frac{18.59\sqrt{2}P_3}{7(3 - 0.936P_1)}. \tag{11}$$

This change amounts to a correction of no more than 5% for the parameters measured.

Since both the retarder angle α and the polarizer angle β may be set independently, there are many possible measurement schemes, involving different sets of measurement angles (α_i, β_i); $i = 1, \ldots, N$, which can be used to determine the Stokes parameters. The relative uncertainty of the measured parameters depends on the choice of the set of measurement angles, and these can be selected to suit one's particular needs. For example, the statistical uncertainty in one parameter may be reduced relative to that of the other two parameters. The usefulness of a particular scheme can be effectively evaluated by a Monte Carlo simulation of a polarization measurement for varying simulated Stokes parameters.

Table 1. Polarization measurement scheme.

Position	1	2	3	4	5	6	7	8	9	10	11	12	13
Electron scattering angle $\theta_e > 10^\circ$													
α (°)	0	22.5	45	67.5	90	112.5	135	67.5	55.5	45	−45	−55.5	−67.5
β (°)	0	22.5	45	67.5	90	112.5	135	22.5	10.5	0	0	−10.5	−22.5
Electron scattering angle $\theta_e \leqslant 10^\circ$													
α (°)	0	22.5	45	67.5	90	112.5	135	67.5	55.5	45	135	145.5	157.5
β (°)	0	22.5	45	67.5	90	112.5	135	22.5	10.5	0	0	−10.5	−22.5

The scheme we have used comprises 13 different polarizer/retarder angle combinations as shown in table 1. Greater emphasis was put on accurate determination of $\bar{P}_3$ than on determination of $\bar{P}_1$ or $\bar{P}_2$. At low scattering angles ($\theta \leqslant 10^\circ$) the scheme was modified to slightly reduce the relative uncertainty of the latter parameters.

A linear least-squares fit of the measured coincidence rates to equation (6) was used to determine Stokes parameters P_1, P_2 and P_3. These were in turn used to calculate the reduced Stokes parameters (using (11)) and P^+ (using (3)). All statistical uncertainties were evaluated by a Monte Carlo method and were found to be consistent with the results of the standard analytical error analysis based on Poisson statistics.

As a matter of course in these measurements it is also possible to measure approximately the corresponding non-coincident Stokes parameters S_1, S_2 and S_3 (i.e. Stokes parameters for the decay radiation averaged over all electron scattering angles). These were measured simultaneously with the coincident parameters. This provides an important experimental check of systematics, in particular, of any system misalignment since S_2 and S_3 are required to be zero by virtue of the axial symmetry of the measurement. All measurements reported here were supported by measured S_2 and S_3 values in the ± 0.01 range. Less importance was attributed to the absolute value of S_1. In our set-up the ability to measure S_1 is impaired by the fact that the retarder in the polarization analyser is calibrated only at 121.6 nm. The non-coincidence photon flux was subject to molecular contamination (photons originating from molecular excitation) and included also other wavelengths. We recorded values of S_1 in the 0.075–0.12 range, compared with the established experimental value of 0.12 ± 0.02 [25]. Coincidence measurements were not subject to this problem.

The possibility of Lyman-α resonance trapping was tested at low electron scattering angles by changing the atomic target density by a factor of 3 and looking for variation in the measured Stokes parameters. No significant variation was observed.

3. Results and discussion

Directly measured Stokes parameters and the reduced Stokes parameters derived from these are presented in table 2. Errors here represent statistical uncertainties combined with the uncertainty in the measured polarization efficiency P, and are quoted at one standard deviation. Figures 5–7 show graphs of the Stokes parameters compared to various experimental data and a single theoretical curve (CCC calculation of Bray and Stelbovics [11]). The linear parameters $\bar{P}_1$ and $\bar{P}_2$ are also presented through equivalent parameters P_l (linear polarization) and γ (charge cloud alignment angle), in figures 8 and 9. The two sets of parameters are related by [18]

$$P_l = \sqrt{\bar{P}_1{}^2 + \bar{P}_2{}^2}, \qquad \gamma = \tfrac{1}{2} \arg(\bar{P}_1 + \mathrm{i}\bar{P}_2). \tag{12}$$

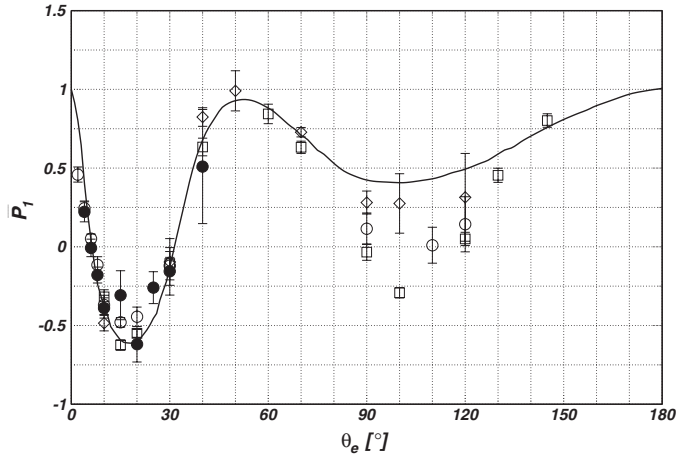

Figure 5. Reduced Stokes parameter $\bar{P}_1$ as a function of the electron scattering angle θ_e. The reported polarization correlation measurements (●) are compared with those deduced from the angular correlation measurements of Williams (□) [9] and Yalim *et al* (◇) [7], as well as polarization correlation measurements of O'Neill *et al* (○) [8]. Error bars represent statistical uncertainties quoted at one standard deviation. Also shown are the 70 state convergent close coupling results of Bray and Stelbovics (——) [11].

Table 2. Measured Stokes parameters and derived reduced Stokes parameters as a function of the electron scattering angle θ_e. Errors in brackets are on the last shown digits of their respective numbers.

θ_e (°)	P_1	P_2	P_3	$\bar{P}_1$	$\bar{P}_2$	$\bar{P}_3$	P^+
4	0.190(21)	−0.170(21)	−0.070(20)	0.222(64)	−0.527(63)	−0.093(27)	0.584(64)
6	0.114(19)	−0.232(19)	−0.032(19)	−0.007(56)	−0.701(56)	−0.042(24)	0.705(55)
8	0.055(18)	−0.276(18)	−0.098(17)	−0.180(51)	−0.819(53)	−0.125(22)	0.850(51)
10	−0.020(24)	−0.250(24)	−0.096(18)	−0.389(65)	−0.724(71)	−0.120(23)	0.834(63)
15	−0.008(57)	−0.243(58)	−0.191(44)	−0.31(16)	−0.71(17)	−0.240(55)	0.83(15)
20	−0.108(44)	−0.230(44)	−0.204(35)	−0.62(12)	−0.65(13)	−0.247(42)	0.94(10)
25	0.026(37)	−0.215(37)	−0.307(28)	−0.26(10)	−0.63(11)	−0.388(35)	0.80(9)
30	0.063(53)	−0.128(53)	−0.277(41)	−0.16(15)	−0.38(16)	−0.354(53)	0.58(11)
40	0.28(11)	−0.09(11)	−0.125(85)	0.51(36)	−0.28(36)	−0.17(12)	0.73(33)

The $\bar{P}_1$ and $\bar{P}_2$ results reported here are in good agreement with earlier measurements of O'Neill *et al* [8], carried out in this laboratory. O'Neill *et al* measured P_1 and P_2 both for low ($\leqslant 40^\circ$) and high ($\geqslant 90^\circ$) electron scattering angles using a single reflection linear polarization analyser (without a retarder). It is reassuring that the agreement between our results and their low angle results is good, since the apparatus was significantly modified between these two measurements. Changes made to the system included: replacing the old single mirror polarizer with an entirely new polarization analyser, replacing the electron gun with a new instrument based on the design of Bernius *et al* [26], replacing the discharge tube of the H-source and redesigning its shielding, and improving stability and tunability of the bias voltages on the elements of the electron gun and the electron energy. The consistency of both sets of results strongly supports the essential validity of our measurement method.

Both sets of results exhibit a polarization reduction below theoretical predictions at low scattering angles ($\leqslant 10^\circ$). This is most likely caused by finite volume and solid angle

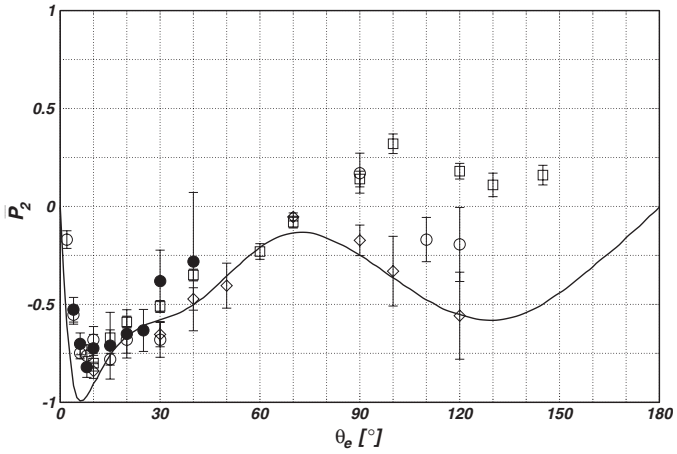

Figure 6. Reduced Stokes parameter $\bar{P}_2$ as a function of the electron scattering angle θ_e. Symbols are the same as in figure 5.

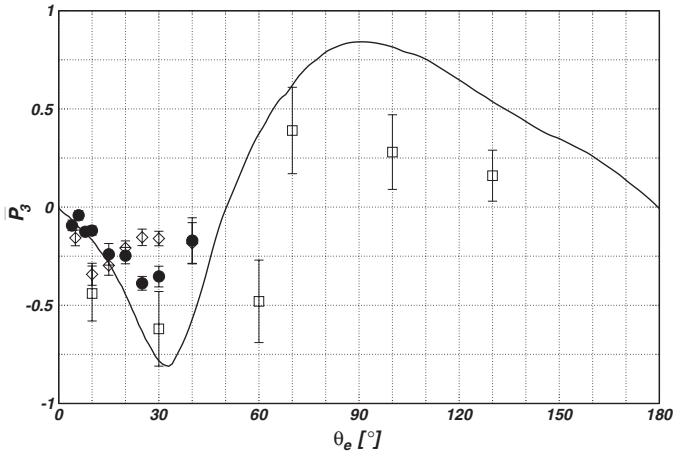

Figure 7. Reduced Stokes parameter $\bar{P}_3$ as a function of the electron scattering angle θ_e. The reported polarization correlation measurements (●) are compared with polarization correlation earlier results of measurements of Williams (□) [16] and Nic Chormaic *et al* (◇) [17]. Other details as in figure 5.

effects. The finite size of the interaction region, and the finite acceptance angle of the electron detector, which cannot be avoided in a real experiment, result in the measurement necessarily averaging over a range of scattering geometries, which can lead to a reduction of the measured polarization. This effect is particularly important at low electron scattering angles, because a small change of scattering geometry can significantly affect both the values of the coherence parameters and the differential cross-section. The finite volume effect was studied numerically by van der Burgt *et al* [27], and more recently by Humphrey [28, 29]. Both these authors showed that the finite size of the interaction region generally contributes to a reduction of the measured polarization particularly at very low electron scattering angles. Humphrey also showed [28] that the size of the acceptance solid angle of the electron detector has a distinct effect on the measured polarization under these experimental conditions. It is worth noting

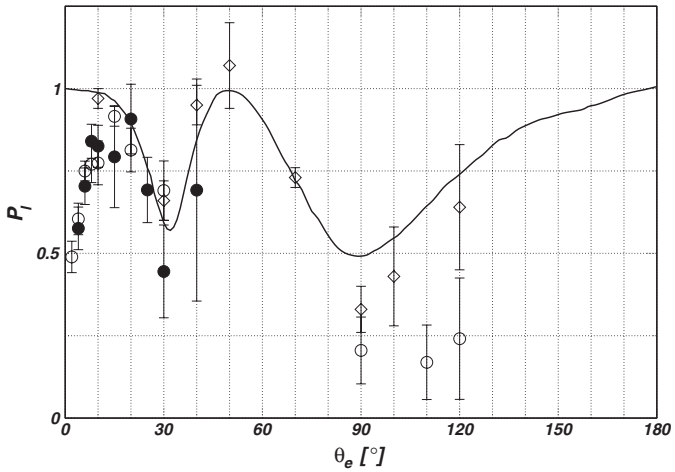

Figure 8. Linear polarization P_l as a function of the electron scattering angle θ_e. Symbols are the same as in figure 5. The results of Williams are not shown here to improve readibility.

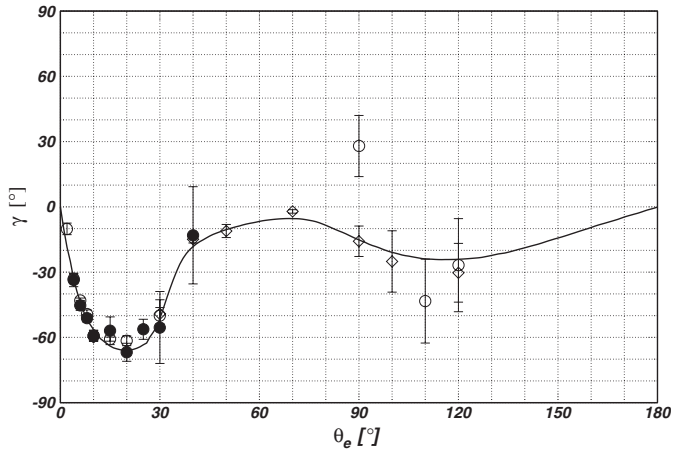

Figure 9. Charge cloud alignment angle γ as a function of the electron scattering angle θ_e. Other details as in figure 8.

that the charge cloud alignment angle γ displays much lower sensitivity to these effects of the experimental geometry at low angles, than the linear polarization P_l, as can be seen in figures 8 and 9.

The new $\bar{P}_3$ results (figure 7) are in disagreement with the CCC theory (and other modern calculations) for electron scattering angles $\theta_e \geqslant 20^\circ$. The data follow the trend of the theoretical P_3 curve, but the measured values are approximately 40% lower (in terms of absolute value) than the CCC predictions. Figure 10 illustrates the observed disagreement between the measured coincidence signal, as a function of the analyser settings, and the prediction of the CCC theory, with the details of our experimental geometry accounted for, at the electron scattering angle of 30°. This provides a direct comparison between the measurement and the theory, similar to angular correlation curves. The theoretical data are normalized to the same total detected photon flux as the measured coincidence rates. The

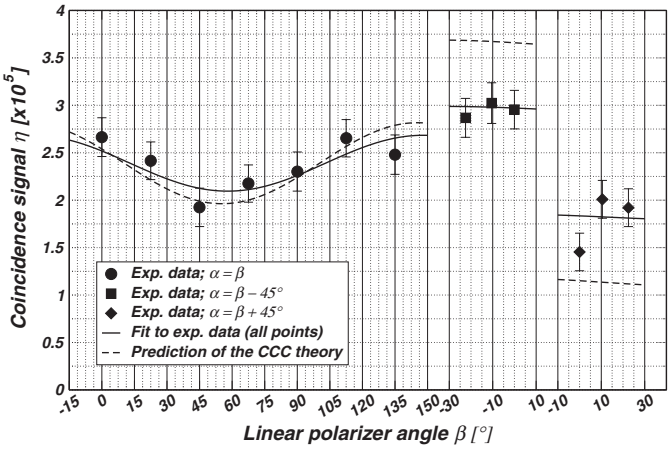

Figure 10. Measured coincidence signal η as a function of the orientation of the elements of the polarization analyser, for the electron scattering angle of 30°; (——) is the least-squares fit, while (- - - -) represents the prediction of the CCC theory [11] for our experimental geometry. α is the retarder angle.

normalization factor appears in equation (6) as $I_0 t_p t_r$, and is determined in the fitting procedure along with P_1, P_2 and P_3.

The initial polarization correlation measurements of $\bar{P}_3$ reported by Williams [16] are in rather poor agreement with the new results at 10° and 30°, but because of his large error bars it is difficult to draw any conclusions. The results of Nic Chormaic *et al* [17] seem to follow a completely different trend. It is possible that these results suffered from a systematic error caused by an error in evaluating the retardance of their Lyman-α quarter-wave plate. Nic Chormaic *et al* did not perform any calibration of retardance in their system, but relied on the reports from other groups using similar retarders, and the manufacturer's specification. It is our experience that these cannot be completely relied on.

It is not clear why our results rather seriously deviate from modern theories in P_3, while the agreement for P_1 and P_2 is relatively good. Figure 10 shows explicitly that the observed discrepancy is restricted to P_3, and appears to be caused by a depolarization effect that emerges as reduced modulation of the coincidence signal when the polarizer and the retarder axes are not set parallel to each other. The most obvious possible explanation might be that there was a serious discrepancy between the actual value of the phase shift of the retarder Δ and the value used during analysis of the results. This was ruled out because we calibrated the plate carefully before the measurements and we also verified the value of Δ several times during the course of the polarization correlation measurements. We always recorded retardance consistent with the initial calibration. These occasional cross-checks were not performed with the same accuracy as the initial calibration, but they ruled out any significant change of Δ.

Other instrumental factors, such as possible small misalignment of the optical elements, or uncertainty in the value of the polarisance and the retardance, cannot be used to explain the observed deviation in $\bar{P}_3$. We estimate that their effects combine to approximately 3% systematic error, significantly smaller than statistical uncertainty of our measurements. We also made sure that our results were not significantly affected by radiation trapping, which could reduce the measured polarization. Humphrey [28] studied other possible sources of systematic errors in crossed beam experiments. His results strongly suggest that factors such as spread of propagation angle in the electron beam or a small displacement of the electron analyser do not significantly influence the outcome of polarization correlation measurements.

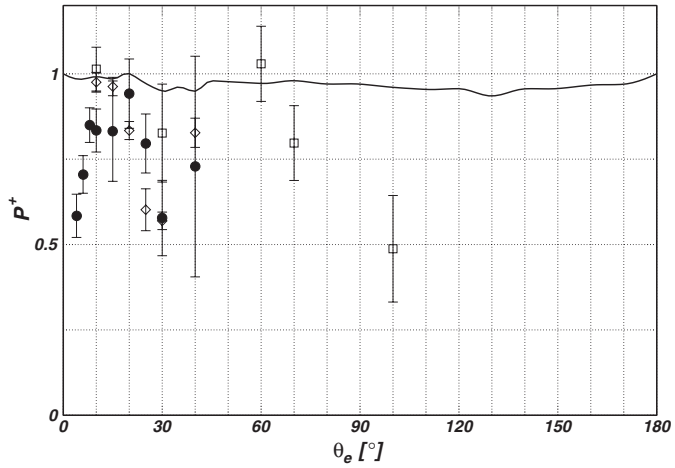

Figure 11. Excitation coherence parameter P^+ as a function of the electron scattering angle θ_e. The reported polarization correlation measurements (●) are compared with P^+ calculated based on $\bar{P}_3$ measurements of Williams (□) [16] and Nic Chormaic *et al* (◇) [17], combined with the weighted average of available $\bar{P}_1$ and $\bar{P}_2$ data (see table 3). Other details as in figure 5.

The outcome of the measurements of the electron impact excitation of H(2p) could, in principle, also be affected by a contribution from collisionally excited H(2s). These states cannot be resolved by electron energy analysis, but H(2s) cannot directly decay to the ground state by emission of a Lyman-α photon. Therefore, our electron–photon coincidence measurements should not be directly affected. In an external electric field, however, H(2s) and H(2p) states are mixed (linear Stark effect), and atoms excited to the nominally 2s state can decay through its 2p admixture. We made sure that stray electric fields in the interaction region were kept to a minimum by shielding all their possible sources. This minimized the extent of 2s–2p mixing. In addition, in the range of electron scattering angles θ_e covered by our measurements, and at 54.4 eV, the ratio of the differential cross-sections for the excitation of H(2s) and H(2p) $\sigma(2s)/\sigma(2p)$ (measured by Williams [9]) is significantly lower than 1 (maximum of 0.4 at 40°). The above allows us to conclude that our results were not in any significant way affected by a contribution from atoms excited to the 2s state.

Taking all this into account, we have to believe that our $\bar{P}_3$ results are essentially valid. This leaves open the question of the source of the deviation between the theory and the measurement for this parameter. It is worth noting that a similar deviation of measured $\bar{P}_3$ from theory has recently been observed by Brown *et al* [30] for electron impact excitation of the $3^1\,P_1$ state of Mg by 40 eV electrons ($\lambda = 285.2$ nm), although these authors attributed the discrepancy to some unknown experimental artefact. Also measurements of the polarization of Lyman-α light resulting from a cascade from collisionally excited 3^2 D states of hydrogen, performed by Farrell *et al* [31] and Kumar *et al* [32], displayed much lower P_3 than theoretically predicted.

The P^+ parameter is of particular importance, as it can be used to quantify the coherence of spin-unresolved electron impact excitation, and thus, indirectly, probes the importance of spin exchange during the collision. We were able to measure all coherence parameters needed to determine P^+ in a single measurement, under the same experimental conditions. This should positively influence the quality of the results. In fact our Monte Carlo data analysis procedure directly determines P^+ and its uncertainty from experimental data, without analysing the statistics of individual Stokes parameters first. The covariances of the parameters of the fit are automatically taken into account. Figure 11 shows the measured values of P^+ along with

Table 3. Sources of experimental data used to calculate P^+. Average P_l is a weighted average of the available $P_l = \sqrt{P_1^2 + P_2^2}$ data. 'Wg' denotes results of Weigold *et al* (early angular correlation measurements from 1980) [10], 'W81'—Williams (1981) [9], 'Y'—Yalim *et al* (1999) [7], 'ON'—O'Neill *et al* (1998) [8], 'W86'—Williams (1986) [16] and 'NC'—Nic Chormaic *et al* (1993) [17]. $\bar{P}_1$ and $\bar{P}_2$ data of Williams at $\theta_e > 70^\circ$ were not included as it is now accepted generally that they are in error [7].

	Source			Value		
θ_e (°)	P_1, P_2	P_l	P_3	Average P_l	P^+ (W86 P_3)	P^+ (NC P_3)
10	W81, ON	Y	W86, NC	0.913 ± 0.023	1.01 ± 0.07	0.98 ± 0.03
15	W81, ON		NC	0.916 ± 0.023		0.96 ± 0.03
20	W81, ON		NC	0.81 ± 0.03		0.83 ± 0.03
25	Wg		NC	0.582 ± 0.062		0.602 ± 0.061
30	Wg, W81, ON	Y	W86, NC	0.546 ± 0.024	0.83 ± 0.15	0.57 ± 0.03
40	Wg, W81	Y	NC	0.81 ± 0.04		0.827 ± 0.043
60	Wg, W81		W86	0.91 ± 0.06	1.03 ± 0.11	
70	W81	Y	W86	0.695 ± 0.024	0.80 ± 0.11	
100	Wg	Y	W86	0.40 ± 0.14	0.49 ± 0.16	

earlier results, deduced from combinations of separate published measurements (details are given in table 3).

The deviation from the CCC theory at electron scattering angles $\theta_e \leqslant 10^\circ$ is driven by the magnitude of the measured $\bar{P}_1$ and $\bar{P}_2$, presumably due to finite volume effects (discussed above). The agreement at 25° is rather poor, while our measurement at 30° strongly suggests a value of $P^+ < 1$. At both 25° and 30°, the deviation is mostly caused by the measured P_3, which significantly deviates from the theoretical prediction. The significance of these low values of P^+ is not clear as the source of the discrepancy for P_3 is not yet understood.

4. Conclusions

We have reported new measurements of electron impact excitation of 2p states of atomic hydrogen at the benchmark electron energy of 54.4 eV and scattering angles up to 40°. All three reduced Stokes parameters, i.e. $\bar{P}_1$, $\bar{P}_2$ and $\bar{P}_3$ were determined in a single polarization correlation study. Consequently, the excitation coherence parameter P^+, quantifying the importance of spin exchange in this process, has been determined in a single direct measurement for the first time.

The $\bar{P}_1$ and $\bar{P}_2$ results presented in this work are consistent with the earlier measurements and the theoretical predictions. This is entirely as expected. The new $\bar{P}_3$ results, however, deviate significantly from the predictions of all modern theories, in particular the convergent close coupling method of Bray and Stelbovics [11], and also differ from previous experimental results.

All modern theoretical methods predict P^+ essentially equal to unity. The newly measured values of the P^+ parameter suggest less coherent excitation, even at a relatively low scattering angle of 30°. This suggests that under such kinematic conditions spin exchange may play a more significant role than the current theoretical methods predict.

We believe that the observed deviations cannot be explained in terms of known possible sources of systematic errors, such as resonance trapping, misalignment of the system or poorly characterized retardance of the polarization analyser. We also believe that we have excluded the possibility that a contribution from the collisionally excited metastable H(2s) state affects

our H(2p) study. We currently cannot explain the source of the observed deviations in $\bar{P}_3$ and P^+.

The success of the CCC theory, in describing the electron impact excitation of the alkali elements and helium [33], suggests very strongly that this method should adequately describe excitation of hydrogen. The disagreement between the current P_3 results and the CCC theory is therefore very surprising. We believe, however, that, given the care we have taken in making these measurements, the results should not be lightly dismissed. It is important that the source of this discrepancy is fully understood.

Acknowledgments

This work was supported by an Enterprise Ireland Basic Research Grant. M L Gradziel gratefully acknowledges the receipt of a Daniel O'Connell Research Scholarship from NUI Maynooth. The work would not have been possible without the excellent technical support of David Watson and Bill Lanigan.

References

[1] Fursa D V and Bray I 1995 *Phys. Rev.* A **52** 1279
[2] Madison D H, McEachran R P and Lehmann M 1994 *J. Phys. B: At. Mol. Opt. Phys.* **27** 1807
[3] Karaganov V, Bray I, Teubner P J O and Farrell P 1996 *Phys. Rev.* A **54** R9
[4] Bray I 1994 *Phys. Rev.* A **49** 1066
[5] Madison D H, Bartschat K and McEachran R P 1992 *J. Phys. B: At. Mol. Opt. Phys.* **25** 5199
[6] Yalim H A, Cvejanovic D and Crowe A 1997 *Phys. Rev. Lett.* **79** 2951
[7] Yalim H A, Cvejanovic D and Crowe A 1999 *J. Phys. B: At. Mol. Opt. Phys.* **32** 3437
[8] O'Neill R W, van der Burgt P J M, Dziczek D, Bowe P, Chwirot S and Slevin J A 1998 *Phys. Rev. Lett.* **80** 1630
[9] Williams J F 1981 *J. Phys. B: At. Mol. Phys.* **14** 1197
[10] Weigold E, Frost L and Nygaard K J 1980 *Phys. Rev.* A **21** 1950
[11] Bray I and Stelbovics A 1992 *Phys. Rev.* A **46** 6995
[12] Wang Y D, Callaway J and Unnikrishnan K 1994 *Phys. Rev.* A **49** 1854
[13] van Wyngaarden W L and Walters H R J 1986 *J. Phys. B: At. Mol. Phys.* **19** 929
[14] Scholz T T, Walters H R J, Burke P G and Scott M P 1991 *J. Phys. B: At. Mol. Opt. Phys.* **24** 2097
[15] Madison D H, Bray I and Mc Carthy I E 1991 *J. Phys. B: At. Mol. Opt. Phys.* **24** 3861
[16] Williams J F 1986 *Aust. J. Phys.* **39** 621
[17] Nic Chormaic S, Chwirot S and Slevin J 1993 *J. Phys. B: At. Mol. Opt. Phys.* **26** 139
[18] Andersen N, Gallagher J W and Hertel I V 1988 *Phys. Rep.* **165** 1
[19] Blum K and Kleinpoppen H 1979 *Phys. Rep.* **52** 203
[20] Slevin J 1984 *Rep. Prog. Phys.* **47** 461
[21] Born M and Wolf E 1975 *Principles of Optics* (Oxford: Pergamon)
[22] Clarke D and Grainger J F 1971 *Polarised Light and Optical Measurements* (Oxford: Pergamon)
[23] Goeke J, Hanne G F and Kessler J 1989 *J. Phys. B: At. Mol. Opt. Phys.* **22** 1075
[24] Humphrey I 1999 *Meas. Sci. Technol.* **10** 403
[25] Ott W R, Kauppila W E and Fite W L 1970 *Phys. Rev.* A **1** 1089
[26] Bernius M T, Man K F and Chutjian A 1988 *Rev. Sci. Instrum.* **59** 2418
[27] van der Burgt P J M, Corr J J and McConkey J W 1991 *J. Phys. B: At. Mol. Opt. Phys.* **24** 1049
[28] Humphrey I 2001 *Meas. Sci. Technol.* **12** 246
[29] Humphrey I 2002 *Meas. Sci. Technol.* **13** 1341
[30] Brown D O, Cvejanovic D and Crowe A 2003 *J. Phys. B: At. Mol. Opt. Phys.* **36** 3411
[31] Farrell D, Chwirot S, Srivastava R and Slevin J 1990 *J. Phys. B: At. Mol. Opt. Phys.* **23** 315
[32] Kumar M, Stelbovics A T and Williams J F 1993 *J. Phys. B: At. Mol. Opt. Phys.* **26** 2165
[33] Bray I, Fursa D V, Kheifets A S and Stelbovics A T 2002 *J. Phys. B: At. Mol. Opt. Phys.* **35** R117